Evidence for an electromagnon in $GdMn_2O_5$: A multiferroic with a large electric polarization

A. Vaunat,[1,2,3] V. Balédent,[1] S. Petit,[2] P. Roy,[3] J. B. Brubach,[3] G. Giri,[4] E. Rebolini,[4] P. Steffens,[4] S. Raymond,[5] Q. Berrod,[4,6] M. B. Lepetit,[7,4] and P. Foury-Leylekian[1,*]

[1]*Université Paris-Saclay, CNRS, Laboratoire de Physique des Solides, 91405, Orsay, France*
[2]*Laboratoire Léon Brillouin, CEA, CNRS, Université Paris-Saclay, F-91191 Gif-sur-Yvette, France*
[3]*Synchrotron SOLEIL, L'Orme des Merisiers, Saint Aubin BP 48, 91192, Gif-sur-Yvette, France*
[4]*Institut Laue Langevin, 38000 Grenoble, France*
[5]*Université Grenoble Alpes, CEA, IRIG, MEM, MDN, 38000 Grenoble, France*
[6]*CNRS, CEA, IRIG-SyMMES, Université Grenoble Alpes, 38000 Grenoble, France*
[7]*Institut Néel, CNRS, 38042 Grenoble, France*

(Received 4 December 2020; revised 3 March 2021; accepted 23 April 2021; published 28 May 2021)

We report in this paper the dynamical properties of $GdMn_2O_5$ studied by inelastic neutron scattering and infrared spectroscopy assisted by *ab initio* calculations. Our work sheds light on the electromagnon, a magnetic mode that can be excited by an electric field. Combining spin-wave measurements, simulations, and *ab initio* calculations of the single-ion anisotropies and the superexchange interactions, we describe in detail the magnetic contribution to this mode. An exhaustive study of the temperature and polarization dependence of its electroactivity completes this comprehensive study of the complex $GdMn_2O_5$ system.

DOI: 10.1103/PhysRevB.103.174434

Magnetoelectric multiferroics, which simultaneously stabilize magnetic and polar static orders, have been predicted to present unusual dynamical magnetoelectric effects (ME) [1]. The relatively large magnitude of this dynamical ME response [2], as well as its strong interaction with light [2,3], is extremely attractive for potential applications, for example, multifunctional spin-based memories or optical switches, among others. The dynamical ME effects under consideration in this paper are characterized by the existence of an electroactive magnetic excitation called electromagnon. The electroactivity of electromagnons was first observed in type-II multiferroics, where ferroelectricity is magnetically induced. In orthorhombic $RMnO_3$ and RMn_2O_5 (R = Tb, Y) families, both THz [3–6] and Raman [7] spectroscopies showed that this mode can be excited by means of the electric field of light. The demonstration of the complementary magnetic nature of this excitation has been the prerogative of inelastic neutron scattering (INS) [8,9]. Since then, electromagnons have also been reported in type-I multiferroics such as hexagonal $RMnO_3$ [10], in $BiFeO_3$ [11], and even in the paraelectric compound $Ba_2Mg_2Fe_{12}O_{22}$ [12]. To describe this unusual property, different mechanisms were proposed, particularly for the manganite families. These models basically rely on the very same magnetoelectric coupling which accounts for the static properties: lattice vibrations alter the exchange couplings or anisotropies which in turn affect the magnon spectrum. In helical magnetic systems, for instance, where the multiferroicity originates from Dzyaloshinskii-Moriya interaction (DMI), the same DMI has been proposed to explain the origin of the electromagnon [13]. Although later refuted in $DyMnO_3$ [14], such a DMI-based scenario seems to be at play in CuO [15]. Other propositions are based on exchange striction (ES) [16,17], and couple a polar lattice mode to the magnon spectrum [4,18]. So far, these models have been consistent with experimental results in $TbMn_2O_5$ [8,9]. These interpretations tend to reduce the definition of the electromagnon to a hybrid magnon-phonon mode, or, as proposed in $ErMnO_3$, to a mixing between a magnon and an electroactive rare-earth crystal-field transition [19]. In this paper we question this issue and support the idea that electroactivity can be a purely electronic phenomenon. Using IR and INS experiments carried out on the same crystal, we investigate in detail the low-energy excitations in the model system $GdMn_2O_5$ and evidence the presence of an electroactive magnon. Completed by spin-wave simulations and *ab initio* calculations, we point out the absence of either lattice or crystal-field mode, suggesting that another mechanism, purely electronic, is at work in $GdMn_2O_5$. The RMn_2O_5 multiferroic compounds crystallize in the polar Pm space group [20] but present quasisymmetries of the paraelectric $Pbam$ space group. Along the c direction, the structure is composed of chains of $Mn^{4+}O_6$ octahedra, separated by layers of R^{3+} or Mn^{3+} ions. In the (a, b) plane, zigzag chains of $Mn^{4+}O_6$ octahedra and $Mn^{3+}O_5$ square pyramids run along the a axis and are stacked along b (see Fig. 1). $GdMn_2O_5$, like the other members of the family [21], shows an incommensurate magnetic ordering (ICM) below $T_N \simeq 38$ K, with a magnetic propagation wave vector $q_1 = (\frac{1}{2}, 0, 0.28)$. Then, below $T_c \simeq 32$ K, the magnetic order becomes commensurate with a propagation wave vector $q_2 = (\frac{1}{2}, 0, 0)$, accompanied by the largest electric polarization known in type-II multiferroics [22–24]. This strong electric polarization has been ascribed to two cooperative ES mechanisms [17]. As all members of the series, the electric polarization is mainly oriented along the b axis [22–24], even if few studies have recently suggested the existence of small additional components along the a and even the c directions [25,26]. The dynamical

*Corresponding author: pascale.foury@u-psud.fr

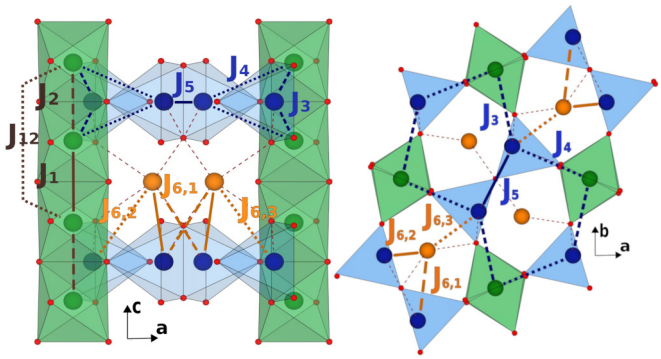

FIG. 1. Structure of $GdMn_2O_5$ in the (a), (c) (left) and (a), (b) plane (right). Mn^{4+} ions are in green, while Mn^{3+} ions are in blue. Oxygens are in red and gadoliniums in orange. Exchange interactions involved in the magnetic ordering and discussed in the text are represented (J_i).

properties of this compound have been studied by means of IR and INS on high-quality single crystals. IR measurements were carried out on the AILES beamline of the SOLEIL synchrotron, with a Bruker IFS125 interferometer [27] equipped with a 4-K closed circle He gaz cryostat and a 1.6 K He pumped bolometer from IRLabs. Figures 2(a) and 2(b) present the absorbance at 5 K for different (e, h) light polarization configurations, calculated using the 40 K measurement as a reference. A very intense peak is visible in the configuration (e, h) = (b, a), with a width of about 1.5 meV (12 cm^{-1}). In the configuration (e, h) = (c, a) where h remains along *a*, this mode disappears, proving its electroactivity for e ∥ b. This result is consistent with observations in the other members of the series [4,9], as the electric polarization stands along the *b* axis. However, it notably differs by its energy, 4.25 meV (34 cm^{-1}), which is well above the sub-meV range generally observed in the other members. Moreover, its large width together with its ill-defined shape may hide several unresolved contributions. Unexpectedly, a sharper peak [FWHM ≈ 0.5 meV (4 cm^{-1})] was found around the same energy for the (e, h) = (a, b) configuration. Here again, the vanishing of the peak for the (e, h) = (c, b) configuration confirms its electroactive nature. The presence of such a mode activated by e ∥ a is unprecedented in this family of compounds. However, it is worth noting that the *Pm* space group allows a nonzero electric polarization along the *a* direction, which may be responsible for this mode. For that matter, a recent polarization experiment evidenced the presence of additional components of P along *a* and even along *c* [24]. If the latter was to be confirmed, the crystallographic group would have to be lowered from *Pm* to *P*1. Figures 2(c) and 2(d) display the temperature dependence of these peaks. Both behave in a similar way: from 5 K up to 30 K, the energy decreases by 1 meV (8 cm^{-1}) while its width increases. No peak could be observed above the magnetic transition at $T_c = 32$ K. We computed the phonon spectra, both in the *Pbam* and *Pm* [Antiferromagnetic (AFM) order, double unit cell] space groups, in order to check for a possible phonon origin of these modes. The calculations were carried out using the first-principles Density Functional Theory frame, a Perdew-Burke-Ernzerhof functional modified for solids functional [28], and the CRYSTAL code [29].

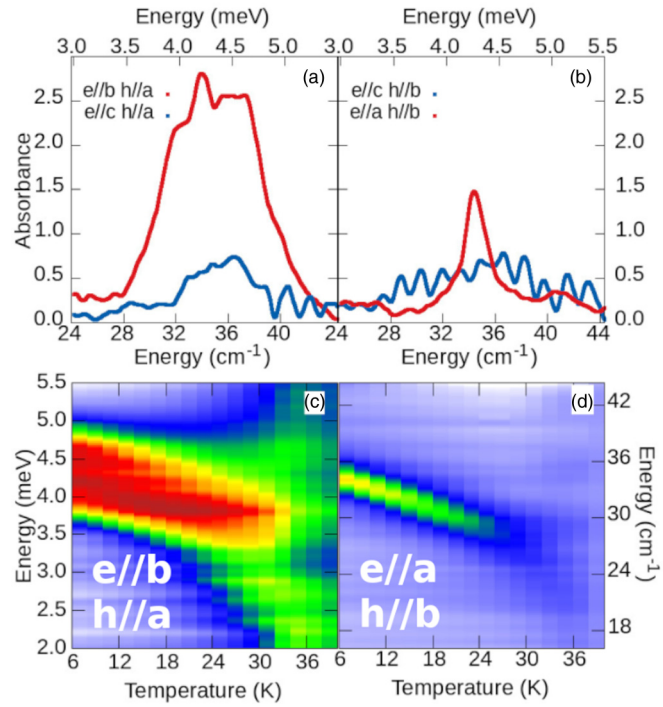

FIG. 2. Absorbance at 5 K with a reference at 40 K in $GdMn_2O_5$ for different orientations of incident *e* and *h* (electric and magnetic field of the light) with respect to the crystallographic axis.

A Monkhorst grid [30] of 8 × 12 × 4 **k**-points was used, a Stuttgart core pseudopotential [31] and the associated basis set [32] was used for the barium atom, while the manganese and oxygen atoms were described using all-electron 3ζ basis sets [33]. The calculations are in good agreement with the phonons measured above 13 meV (≈ 100 cm^{-1}), as shown in the Supplemental Materials [34]. However, no phonon contribution is predicted below 9 meV (≈ 70 cm^{-1}). It thus seems that the detected electroactive low-energy excitation is not related to a phonon, while its appearance at the magnetic transition points toward an electromagnon. We now turn to the investigation of the low-energy spin dynamics. Aiming at avoiding neutron absorption, we used a 80 mg ^{160}Gd-isotope-enriched single crystal synthesized using the standard procedure [35]. INS experiments were performed on the 4F2 (cold) and 2T (thermal) triple axis at Orphée-LLB (France), as well as on the IN6-Sharp, THALES, and IN12 spectrometer (ILL, France). The final wave vector was $k_f = 1.97$ $Å^{-1}$ on 4F2 and 1.5 $Å^{-1}$ on THALES, yielding a resolution of about 0.5 and 0.25 meV, respectively. The magnon dispersion was measured along the H and L directions at 15 K. As can be seen in the color maps of Figs. 3(a) and 3(b), the magnetic spectral weight is maximum at the magnetic zone center with an energy of 4.5 meV, corresponding to the electroactive mode observed in IR spectroscopy. Unexpectedly, the minimum of the dispersion along L is not located at the magnetic zone center (1.5, 0, 0), but significantly shifted close to (1.5, 0, 0.4). This result is all the more intriguing because no elastic magnetic peak can be observed at this particular wave vector down to 5 K. To complete our magnetic study and put constraints on spin dynamics simulations, the sub-meV dispersion was also measured along the L direction. As shown in Fig. 3(c), two modes arise at around

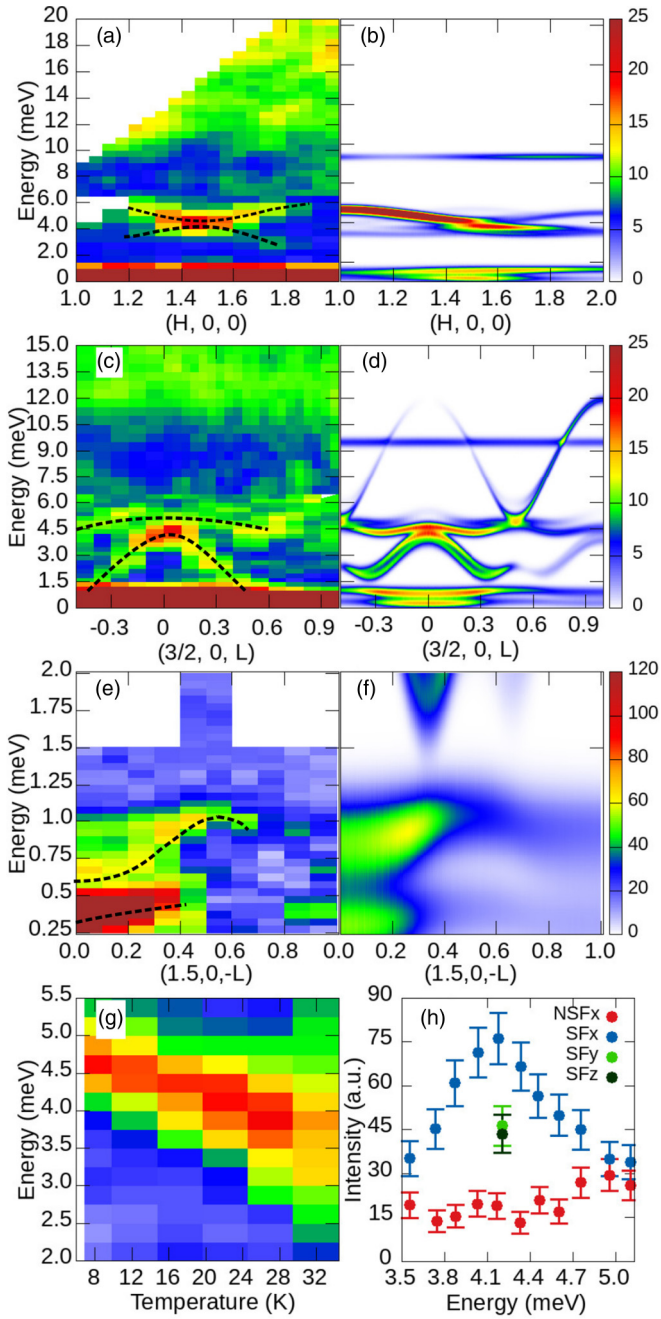

FIG. 3. (a) Inelastic neutron-scattering raw data recorded at 15 K along (H, 0, 0). (c), (e) Inelastic neutron-scattering raw data recorded at 15 K along (3/2, 0, L) performed on the 2-T (E > 6.5 meV) and 4F2 (E < 6.5 meV) spectrometers for (c) and IN12 for (d). (b), (d), and (f) are the associated numerical simulations for (a), (c), and (e), respectively. (f) Evolution of the energy of the $(3/2, 0, L)$ energy scan as a function of temperature to be compared to IR in Figs. 2(c) and 2(d). (h) Inelastic polarized neutron scattering at $Q = (3/2, 0, 0)$ performed at THALES for 15 K. NSFx, SFx SFy, and SFz stands for non-spin-flip, spin-flip with polarization parallel to the a, c, and b crystallographic axes, respectively.

0.3 and 0.7 meV, with a minimum at the magnetic zone center. To evidence any lattice contribution to the spectral weight at 4.5 meV, polarized INS was carried out at the magnetic zone center. The result, shown in Fig. 3(h), demonstrates that the signal is purely magnetic, with no intensity in the non-spin-flip channel. The temperature dependence of the energy of this mode, represented in Fig. 3(d), is strikingly similar to the evolution of the IR mode. It can reasonably be concluded that it is one and the same mode: an electromagnon. To further understand the magnetic contribution to this electromagnon, linear spin-wave theory was employed to simulate the spin dynamics. For $R\mathrm{Mn_2O_5}$, five interactions (labeled $J_{1...5}$) are commonly used to describe the Mn-Mn couplings in the *Pbam* paraelectric group [36]. The *Pbam* to *Pm* weak symmetry breaking is usually neglected. It would lead to four different J_3 and J_4 couplings, two different J_1, J_2, and J_5. Additional interactions between the rare-earth and Mn atoms are also necessary to describe the spin dynamics in the sub-meV range [17,36–38]. Spin-wave calculations have been performed using the software described in [39]. No less than nine different exchange interactions were taken into account, represented in Fig. 1: (i) the five Mn-Mn interactions described above, (ii) the second-neighbor Mn-Mn interaction along the c direction (J_{12}), shown to be important in some $\mathrm{RMn_2O_5}$ compounds [8] and requiring AFM to get the correct dispersion shape of the electromagnon excitation, and (iii) three Gd-Mn interactions. Finally, we added the Mn^{4+} and Mn^{3+} axial anisotropies but neglected the Gd^{3+} anisotropy, as our *ab initio* calculations find it to be negligible. These anisotropies actually stabilize the ferromagnetic arrangement along the c axis ($q_l = 0$). The magnetic frustration along c originates from the competition between the AFM J_{12}, J_4 and the FM J_1, J_2 couplings. The shift of the minimum of the dispersion to L ≈ 0.4 is ascribed to the balance between these competing interactions. In a first attempt, Mn-Gd exchange interactions were neglected. Noteworthy, the hierarchy reported in Refs. [8,9] $J_5 > J_4 > J_1$, along with a small J_3, does not reproduce data agreeing with our *ab initio* calculations (see below). The best result was obtained for a small J_5. Figures 3(b), 3(d) and 3(f) show the result of the simulation for $J_1 = -1.7$ meV (FM); $J_2 = 0.65$ meV (AFM); $J_{12} = 0.74$ meV; $J_{3,1} = J_{3,2} = 0.12$ meV; $J_4 = 2.25$ meV; $J_5 = 0.15$ meV; $\Delta_{Mn4+} = 0.3$ meV, and $\Delta_{Mn3+} = 0.6$ meV. The amplitudes and minima of the two modes corresponding to Mn spin waves agree quite well with the experimental data [dashed lines in Fig. 3(c)]. In addition, the simulation of the dispersion along H is in good agreement with the data [Fig. 3(a)], confirming the validity of our exchange values set. To account for the two low-energy excitation modes close to 0.3 and 0.7 meV [Fig. 3(e)], three additional exchange interactions are necessary between Mn and Gd: $J_{6,1} = 0.1$ meV, $J_{6,2} = 0.1$ meV, and $J_{6,3} = 0.06$ meV. The energy difference between the two low-energy modes is directly related to $J_{6,3}$, which enables an accurate determination of this particular coupling. $J_{6,3}$ can provide an explanation to the different ordered moments measured for the two Gd sites (Gd1 and Gd2 in [17]). Gd2 is indeed in a less favorable configuration than Gd1 regarding $J_{6,3}$; its moment will seek to relocate more than that of Gd1 to have a lower ground state. The unexpected weak value obtained for J_5 calls for a theoretical validation. The main nearest-neighbor Mn-Mn exchange interactions, as well as the Mn and Gd anisotropies, were calculated using *ab initio* calculations. Since theses quantities are essentially local and dominated by the physics of the strongly

correlated electrons at the Fermi level, a thorough treatment of the electron correlation within the magnetic orbitals is required in order to reach an accuracy comparable with experiments. We thus used methods specifically developed to this end. For the magnetic integrals calculations, we used the Selected-Active-Space + Single-excitations [40] (SAS+S) method. This method treats, using exact diagonalization on properly designed embedded fragments, the electronic correlations within the magnetic orbitals, the ligand-to-metal charge transfers that bridge the magnetic interactions, and the screening effect on all the preceding configurations. The anisotropies were computed from similar high-level local spectroscopic calculations. Indeed, it was shown that despite the single-electron character of the spin-orbit coupling, the electron correlation within the magnetic ion orbitals have to be exactly treated for an accuracy comparable with neutrons scattering experiments [41]. We thus used the CAS+DDCI (Complete Active Space (CAS) [42] + Difference Dedicated Configuration Interaction [43–45]) method for the calculation of the ground and excited states without spin orbit. This method ensures that the electronic correlations within the magnetic orbitals, the screening effects up to double excitations, and the spin-orbit effects are thoroughly treated. The obtained states were further coupled by the spin-orbit interaction and the anisotropies determined along the method of Chibotaru and Ungur [46]. The calculations were performed using the MOLCAS package [47], the CASDI code [48], and the RELAXSE [49] codes. The calculations were performed using the room-temperature *Pbam* experimental geometry optimized in the same group. The calculated exchange couplings are $J_1 = -0.43$ meV, $J_2 = -2.36$ meV, $J_3 = 1.13$ meV, $J_4 = 3.98$ meV, $J_5 = 0.62$ meV. As one can see, the order of magnitude and the relative amplitudes of all the exchange interactions are in good agreement with the one inferred from our spin-wave simulations. Most interestingly, the calculated J_5 interaction has also a very weak value, much weaker than J_4 or J_3, and close to the one extracted from the simulations. Such a weak value is unusual within the RMn_2O_5 family, which is depicted as an AFM zigzag chain along the *a* axis generated by strong J_4 and J_5 AFM couplings ($J_4 = 2.9$ and $J_5 = 3.5$ meV in $TbMn_2O_5$, or $J_4 = 3.75$ and $J_5 = 2.75$ meV in YMn_2O_5 [8,9]). One should, however, note that a negligible J_4 has already been evidenced in $PrMn_2O_5$ [35]. Our calculations predict anisotropies greater than those considered until now [8], with $\Delta_{Mn4+} = 0.45$ meV along the octahedra long axis parallel to *b*, and $\Delta_{Mn3+} = 0.9$ meV along the apical direction of the pyramid, but in good agreement with our experimental fits. We now have to emphasize that this electromagnon electroactivity is not carried by any lattice mode or crystal field, as evidenced experimentally. This calls into question the very nature of this excitation. As reported recently [50,51], the total electric polarization results from a combination of both an ionic and an electronic component. The consideration of a purely electronic contribution to ferroelectricity is further reinforced by other experimental results [52], while the exchange striction mechanism occurring below T_N is usually associated to an ionic contribution. In light of this information, our results strongly suggest that the electromagnon in $GdMn_2O_5$ is a purely electronic excitation. In the actual *Pm* space group, four different ferroelectric ground states are predicted [51] in the magnetic phase, corresponding to the four sign combinations for the *a* and *b* components of the polarization. In this picture a change of the magnetic structure modifies the electronic density. As a consequence, charge and spin degrees of freedom can no longer be treated independently. Thus the magnetic excitation described above as a spin wave actually modifies dynamically the orbital part of the wave function. This entanglement would lead to a change in the polarization amplitude visible via IR spectroscopy. This scenario is compatible with the IR polarization selection rule, as both *a* and *b* electronic components exist in the actual *Pm* space group. By neglecting the orbital contribution in our spin-wave model to determine exchange interactions, effective values only are determined, this, and the room-temperature *Pbam* structure used for the calculations, may explain the differences with respect to some calculated *J* values by *ab initio* technique.

In conclusion, our complementary analysis of INS and IR results on $GdMn_2O_5$ highlights a relatively high-energy electromagnon, bearing both magnetic and electroactive signatures. The magnetic contribution can be explained and modeled by the standard linear spin-wave theory with 11 parameters, necessary to match the numerous magnon branches. However, the absence of any lattice or crystal-field contribution on the one hand, and the unusual polarization dependence of the electroactivity on the other hand, call for new modeling. We thus propose a purely electronic excitation where orbital and spin degrees of freedom are no longer decoupled. This picture is strongly supported by recent evidence of an electronic contribution to the usual ionic ferroelectricity [51,52] in this family and may explain the exhaustive experimental results reported here. This framework could be relevant not only in the entire family of RMn_2O_5 but in all magnetoelectric materials.

This study was supported by grants from LLB and SOLEIL, and LabEx PALM through Contract No. ANR-10-LABX-0039-PALM. Experiments at LLB and ILL were sponsored by the French Neutron Federation (2FDN), with Data References 10.5291/ILL-DATA.CRG-2724, 10.5291/ILL-DATA.EASY-496, and 10.5291/ILL-DATA.CRG-2608. We acknowledge SOLEIL for provision of synchrotron radiation facilities (Proposals No. 20170190, No. 20180772, and No. 20191991). We acknowledge the IDRIS and CRIANN computer centers for providing us with computer hours under Projects No. 91842 and No. 2007013, respectively.

[1] G. A. Smolenskii and I. E. Chupis, Soviet Phys. Usp. **25**, 475 (1982).
[2] A. Cano, Phys. Rev. B **80**, 180416(R) (2009).
[3] A. Pimenov, A. A. Mukhin, V. Y. Ivanov, V. D. Travkin, A. M. Balbashov, and A. Loidl, Nat. Phys. **2**, 97 (2006).
[4] A. B. Sushkov, R. V. Aguilar, S. Park, S.-W. Cheong, and H. D. Drew, Phys. Rev. Lett. **98**, 027202 (2007).
[5] A. Pimenov, A. M. Shuvaev, A. A. Mukhin, and A. Loidl, J. Phys.: Condens. Matter **20** 434209 (2008).

[6] Y. Takahashi, R. Shimano, Y. Kaneko, H. Murakawa, and Y. Tokura, Nat. Phys. **8**, 121 (2012).

[7] P. Rovillain, J. Liu, M. Cazayous, Y. Gallais, M.-A. Measson, H. Sakata, and A. Sacuto, Phys. Rev. B **86**, 014437 (2012).

[8] J.-H. Kim, M. A. van der Vegte, A. Scaramucci, S. Artyukhin, J.-H. Chung, S. Park, S.-W. Cheong, M. Mostovoy, and S.-H. Lee, Phys. Rev. Lett. **107**, 097401 (2011).

[9] S. Petit, V. Balédent, C. Doubrovsky, M. B. Lepetit, M. Greenblatt, B. Wanklyn, and P. Foury-Leylekian, Phys. Rev. B **87**, 140301(R) (2013).

[10] S. Pailhès, X. Fabrèges, L. P. Régnault, L. Pinsard-Godart, I. Mirebeau, F. Moussa, M. Hennion, and S. Petit, Phys. Rev. B **79**, 134409 (2009).

[11] P. Rovillain, R. de Sousa, Y. Gallais, A. Sacuto, M. A. Méasson, D. Colson, A. Forget, M. Bibes, A. Barthélémy, and M. Cazayous, Nat. Mater. **9**, 975 (2010).

[12] N. Kida, Y. Ikebe, Y. Takahashi, J. P. He, Y. Kaneko, Y. Yamasaki, R. Shimano, T. Arima, N. Nagaosa, and Y. Tokura, Phys. Rev. B **78**, 104414 (2008).

[13] H. Katsura, A. V. Balatsky, and N. Nagaosa, Phys. Rev. Lett. **98**, 027203 (2007).

[14] N. Kida, D. Okuyama, S. Ishiwata, Y. Taguchi, R. Shimano, K. Iwasa, T. Arima, and Y. Tokura, Phys. Rev. B **80**, 220406 (2009).

[15] K. Cao, F. Giustino, and P. G. Radaelli, Phys. Rev. Lett. **114**, 197201 (2015).

[16] L. C. Chapon, G. R. Blake, M. J. Gutmann, S. Park, N. Hur, P. G. Radaelli, and S.-W. Cheong, Phys. Rev. Lett. **93**, 177402 (2004).

[17] G. Yahia, F. Damay, S. Chattopadhyay, V. Balédent, W. Peng, S. W. Kim, M. Greenblatt, M.-B. Lepetit, and P. Foury-Leylekian, Phys. Rev. B **97**, 085128 (2018).

[18] A. B. Sushkov, M. Mostovoy, R. V. Aguilar, S. W. Cheong, and H. D. Drew, J. Phys.: Condens. Matter **20**, 434210 (2008).

[19] L. Chaix, S. de Brion, S. Petit, R. Ballou, L.-P. Regnault, J. Ollivier, J.-B. Brubach, P. Roy, J. Debray, P. Lejay, A. Cano, E. Ressouche, and V. Simonet, Phys. Rev. Lett. **112**, 137201 (2014).

[20] V. Balédent, S. Chattopadhyay, P. Fertey, M. B. Lepetit, M. Greenblatt, B. Wanklyn, F. O. Saouma, J. I. Jang, and P. Foury-Leylekian, Phys. Rev. Lett. **114**, 117601 (2015).

[21] P. G. Radaelli and L. C. Chapon, J. Phys.: Condens. Matter **20**, 434213 (2008).

[22] N. Lee, C. Vecchini, Y. J. Choi, L. C. Chapon, A. Bombardi, P. G. Radaelli, and S.-W. Cheong, Phys. Rev. Lett. **110**, 137203 (2013).

[23] A. Inomata and K. Kohn, J. Phys.: Condens. Matter **8**, 2673 (1996).

[24] B. Khannanov, E. I. Golovenchits, and V. A. Sanina, J. Phys.: Conf. Series **572**, 012046 (2014).

[25] B. Khannanov, E. I. Sanina, V. A. Golovenchits, and S. M. P., Pis'ma v ZhETF **103**, 274 (2016).

[26] V. A. Sanina, E. I. Golovenchits, B. K. Khannanov, M. P. Scheglov, and V. G. Zalesskii, Soviet J. Exp. Theor. Phys. Lett. **100**, 407 (2014).

[27] P. Roy, M. Rouzieres, Z. Qi, and O. Chubar, Inf. Phys. Technol. **49**, 139 (2006).

[28] J. P. Perdew, A. Ruzsinszky, G. I. Csonka, O. A. Vydrov, G. E. Scuseria, L. A. Constantin, X. Zhou, and K. Burke, Phys. Rev. Lett. **100**, 136406 (2008).

[29] R. Dovesi, A. Erba, R. Orlando, C. M. Zicovich-Wilson, B. Civalleri, L. Maschio, M. Rérat, S. Casassa, J. Baima, S. Salustro, and B. Kirtman, WIREs Comput. Mol. Sci. **8**, e1360 (2018).

[30] H. J. Monkhorst and J. D. Pack, Phys. Rev. B **13**, 5188 (1976).

[31] A. S. M. Dolg, H. Stoll, and H. Preuss, Theor. Chim. Acta **75**, 173 (1989).

[32] M. Dolg, H. Stoll, and H. Preuss, Theor. Chim. Acta **85**, 441 (1993).

[33] D. V. O. M. F. Peintinger and T. Bredow, J. Comput. Chem. **34**, 451 (2012).

[34] See Supplemental Material at http://link.aps.org/supplemental/10.1103/PhysRevB.103.174434 for the calculations of the phonons.

[35] C. Doubrovsky, G. André, A. Gukasov, P. Auban-Senzier, C. R. Pasquier, E. Elkaim, M. Li, M. Greenblatt, F. Damay, and P. Foury-Leylekian, Phys. Rev. B **86**, 174417 (2012).

[36] S. Chattopadhyay, S. Petit, E. Ressouche, S. Raymond, V. Balédent, G. Yahia, W. Peng, J. Robert, M. B. Lepetit, M. Greenblatt, and P. Foury-Leylekian, Sci. Rep. **7**, 14506 (2017).

[37] Y. F. Popov, A. M. Kadomtseva, G. P. Vorob'ev, S. S. Krotov, K. I. Kamilov, and M. M. Lukina, Phys. Solid State **45**, 2155 (2003).

[38] S. Chattopadhyay, S. Petit, E. Ressouche, V. Balédent, S. Raymond, G. Yahia, W. Peng, J. Robert, M. Greenblatt, and P. Foury-Leylekian (unpublished).

[39] S. Petit, Collection SFN **10**, 449 (2010).

[40] A. Gellé, J. Varignon, and M.-B. Lepetit, Europhys. Lett. **88**, 37003 (2009).

[41] K. Ridier, A. Mondal, C. Boilleau, O. Cador, B. Gillon, G. Chaboussant, B. L. Guennic, K. Costuas, and R. Lescouezec, Angew. Chem. Int. Ed. **55**, 3963 (2016).

[42] B. O. Roos, P. R. Taylor, and P. E. Sigbahn, Chem. Phys. **48**, 157 (1980).

[43] J. Miralles, J. P. Daudey, and R. Caballol, Chem. Phys. Lett. **198**, 555 (1992).

[44] V. M. García, O. Castell, R. Caballol, and J. P. Malrieu, Chem. Phys. Lett. **238**, 222 (1995).

[45] V. M. García, M. Reguero, and R. Caballol, Theor. Chem. Acc. **98**, 50 (1997).

[46] L. F. Chibotaru and L. Ungur, J. Chem. Phys. **137**, 064112 (2012).

[47] F. Aquilante, J. Autschbach, R. K. Carlson, L. F. Chibotaru, M. G. Delcey, L. D. Vico, I. F. Galván, N. Ferré, L. M. Frutos, L. Gagliardi, M. Garavelli, A. Giussani, C. E. Hoyer, G. L. Manni, H. Lischka, D. Ma, P. A. Malmqvist, T. Müller, A. Nenov, M. Olivucci *et al.*, J. Comp. Chem. **37**, 506 (2016).

[48] D. Maynau (private communication).

[49] E. Rebolini and M. Lepetit (private communication).

[50] X. Li, S. Zheng, L. Tian, R. Shi, M. Liu, Y. Xie, L. Yang, N. Zhao, L. Lin, Z. Yan, X. Wang, and J. Liu, Chin. Phys. B **28**, 027502 (2019).

[51] J.-Q. Dai, J. Yuan, and C. Ke, J. Magn. Magn. Mater. **516**, 167373 (2020).

[52] S. Partzsch, S. B. Wilkins, J. P. Hill, E. Schierle, E. Weschke, D. Souptel, B. Büchner, and J. Geck, Phys. Rev. Lett. **107**, 057201 (2011).